INVESTIGATION OF SPECTRAL PROPERTIES

OF A DFB LASER SOURCE

by

GOKUL KRISHNA SRINIVASAN

Presented to the Faculty of the Graduate School of

The University of Texas at Arlington in Partial Fulfillment

of the Requirements

for the Degree of

MASTER OF SCIENCE IN ELECTRICAL ENGINEERING

THE UNIVERSITY OF TEXAS AT ARLINGTON

December 2012

Acknowledgements

I would like to thank Prof. Vasilyev for his valuable guidance during the course of my thesis. It was a great experience working under his guidance in the Nonlinear Optics lab.

I thank Prof. Weidong Zhou and Prof. Donald Butler for being on my thesis committee.

I thank my group mate Lu for helping me setup the experiment, and I also thank all of my group mates for being very supportive and encouraging.

I would also like to thank my family and friends for their continued support and wisdom.

December 07, 2012

Abstract

INVESTIGATION OF SPECTRAL PROPERTIES

OF A DFB LASER SOURCE

Gokul Krishna Srinivasan, M.S.

The University of Texas at Arlington, 2012

Supervising Professor: Micheal Vasilyev

We determine the linewidth characteristic of a DFB laser source by conducting experiments employing a coherent detection setup. We use an instrument grade external semiconductor laser device as the local oscillator and the DFB laser as the signal. We analyze the photocurrent using real-time oscilloscope and RF spectrum analyzer.

We compute the auto-correlation and the power spectral density of the photocurrent. We model the natural width of the DFB and compare the simulated plot with the experiment data. We determine the intrinsic linewidth of the DFB laser source with this plot.

We design a LabView program to record the beat center frequency as a function of time while both the lasers are not modulated. With this data, we determine the slow moving drift and the fast fluctuations of the beat frequency.

With these values, it is possible to improve the stability of the DFB laser by designing a feedback loop that would mitigate the drift in the laser source.

Table of Contents

Acknowledgements iii

Abstract iv

List of Illistrations.....vi

Chapter 1 Introduction 1

Chapter 2 Theoretical Background 3

Coherent Detection.....3

Auto-correlation Function.....5

Power Spectral Density.....6

On-Off Keying.....7

Return to Zero.....7

Non-Return to Zero.....8

Chapter 3 Experiment and Results…….....9

Both lasers are not modulated….....9

Modulated DFB and continuous wave local oscillator.....18

Chapter 4 Conclusion.....29

References.....31

Biographical Information.....32

List of Illustrations

Figure 2.1: A binary signal encoded using rectangular pulse amplitude modulation with polar return-to-zero code (taken from Ref. 6])....7

Figure 2.2: A binary signal encoded using rectangular pulse amplitude modulation with polar non-return-to-zero code (taken from Ref. [6])....8

Figure 3.1: Schematic diagram of the experimental setup....9

Figure 3.2: Auto-correlation function of the photocurrent....10

Figure 3.3: Expanded first 2 μs of the auto-correlation function....11

Figure 3.4: Fourier transform of the auto-correlation function....11

Figure 3.5: Data of Figure 3.4 in the vicinity of the signal-LO beat frequency....12

Figure 3.6: Data of Figure 3.4 on logarithmic scale....13

Figure 3.7: Fitting the data with a superposition of two Lorentzian curves....14

Figure 3.8: Beat note between the two lasers (both not modulated)....15

Figure 3.9: Fluctuations and drift of the beat frequency versus time....16

Figure 3.10: The fast, zero-mean fluctuations of the beat center frequency....17

Figure 3.11: Histogram of the fast fluctuations of beat frequency....18

Figure 3.12: Experiment setup with modulated DFB laser....18

Figure 3.13: Optical spectra for RZ-modulated case....20

Figure 3.14: RF Spectra for RZ-modulated case. Peak labels correspond to the beatings between LO and DFB tones marked in Figure 3.13....21

Figure 3.15: Beat peak 2′ at 15.43 GHz for PRBS length of 2^{31}–1....22

Figure 3.16: Beat peak 2′ at 15.43 GHz for PRBS length of 2^{7}–1....23

Figure 3.17: Beat peak 1′ at 4.6 GHz for PRBS length of 2^{31}–1....24

Figure 3.18: Beat peak 1′ at 4.6 GHz for PRBS length of 2^7–1.....25

Figure 3.19: Optical Spectra for NRZ-modulated case. Peak label corresponds to the beating between LO and DFB tones marked in Figure 3.20.....26

Figure 3.20: RF spectra for NRZ-modulated case.....27

Figure 3.21: Beat peak 1 at 11.21 GHz for PRBS length of 2^7–1.....28

Chapter 1

Introduction

The linewidth of a laser is the width (typically the full width at half-maximum, FWHM) of its optical spectrum. It is also the width of the power spectral density of the emitted electric field in terms of frequency, wavenumber or wavelength. The linewidth of a laser is related to the temporal coherence, characterized by the coherence time τ or coherence length $c\tau$ [1].

Determining the linewidth of a laser device is very critical in order to characterize and stabilize a laser. The laser device tends to have drift in the center frequency. This drift can be classified as fast fluctuation, and a slow moving drift. By determining these two parameters, it is possible to find out the drifting pattern of the laser which can further be compensated either while making the measurements or by using an algorithm in the post experimental phase.

Lasers with very narrow linewidth (high degree of monochromaticity) are required for various applications, e.g. as light sources for various kinds of fiber-optic sensors, for spectroscopy, for remote sensing (e.g. LIDAR), in coherent optical fiber communications, and for test and measurement purposes [1].

A laser linewidth can be measured in different ways [1]:

- For large linewidths (> 10 GHz), traditional techniques of optical spectrum analysis, e.g. based on diffraction gratings, are suitable. Another technique is to convert frequency fluctuations to intensity fluctuations, using a frequency discriminator.

- For single-frequency lasers, the self-heterodyne technique is often used, which involves recording a beat note between the laser output and a frequency-shifted and delayed version of it.

For sub-kilohertz linewidths, the ordinary self-heterodyne technique is just not enough, but it can be extended by using a re-circulating fiber loop with an internal fiber amplifier. It is possible to obtain very high resolution by recording a beat note between two independent lasers.

A frequency reference is always needed for optical measurements. For lasers with narrow linewidth, only an optical reference can give a sufficiently accurate reference. The self-heterodyne technique is a way to derive the frequency reference from the device under test itself by applying a large enough time delay, avoiding any temporal coherence between the original beam and the delayed version. Therefore, long fibers are often used. Most laser applications, including high-resolution spectroscopy, optical remote sensing, cooling/trapping, and optical fiber communications, are highly dependent on a laser's spectral performance [2].

The subject of this thesis work is to determine the linewidth of a DFB laser source by analyzing the spectral properties of the beating pattern between a DFB laser and an ANDO laser.

Chapter 2

Theoretical Background

Coherent Detection

Coherent detection is the process of beating an incoming signal with a reference light from a laser source called local oscillator (LO). If the frequencies of the signal and LO are different, the detection is known as optical heterodyne detection, if they coincide – as optical homodyne detection. Coherent detection enables extremely high resolution spectroscopy and can produce high resolution spectra with multiple channels.

Photocurrent can be written as :

$$i(t) = AI(t)R\,, \tag{1}$$

where $i(t)$ is the photocurrent (Amperes), A is the detector's area (m^2), $I(t)$ is the light intensity (W/m^2), and R is the detector's responsivity (Amperes/W). R is given by the equation

$$R = \frac{\eta e}{h\upsilon}. \tag{2}$$

$I(t)$ can be written as

$$I(t) = 2\varepsilon_0 c\left|E(t)\right|^2, \tag{3}$$

where electric field $E(t)$ is represented by equation(4)

$$E(t) = E_S e^{-i\omega_s t} + E_{\mathrm{LO}} e^{-i\omega_{LO} t}. \tag{4}$$

Assuming E_{LO} to be real and constant, we have

$$\begin{aligned}\left|E(t)\right|^2 &= \left|E_S\right|^2 + E_{\mathrm{LO}}^2 + E_S E_{\mathrm{LO}} e^{-i(\omega_S-\omega_{\mathrm{LO}})t} + E_S^* E_{\mathrm{LO}} e^{i(\omega_S-\omega_{LO})t} \\ &= \left|E_S\right|^2 + E_{\mathrm{LO}}^2 + 2E_{\mathrm{LO}}\,\mathrm{Re}\left[E_S e^{-i(\omega_S-\omega_{\mathrm{LO}})t}\right]\end{aligned} \tag{5}$$

where E_S and E_{LO} are the electric fields of the signal and local oscillator, respectively, and ω_S and ω_{LO} are their angular frequencies. Intensity of the combined field can be written as

$$I(t) = I_S + I_{\mathrm{LO}} + 2\sqrt{I_S I_{\mathrm{LO}}}\cos\left[(\omega_S - \omega_{\mathrm{LO}})t\right], \tag{6}$$

where I_S and I_{LO} are the intensities of the signal and local oscillator, respectively. By combining Equations (1), (3), and (5), we obtain photocurrent in the following form:

$$i(t) = C_1 + C_2\left[E_S e^{-i(\omega_S-\omega_{\mathrm{LO}})t} + E_S^* e^{i(\omega_S-\omega_{\mathrm{LO}})t}\right], \tag{7}$$

where C_1 and C_2 are constants. Auto-correlation function of the photocurrent is therefore

$$\left\langle i(t)i(t-\tau)\right\rangle_t = C_1^{\,2} + C_2^{\,2}\left\langle XY\right\rangle_t, \tag{8}$$

where angle brackets stand for averaging over *t*, and

$$\begin{aligned} X &= \left[E_S(t)e^{-i(\omega_S-\omega_{\mathrm{LO}})t} + E_S^*(t)e^{i(\omega_S-\omega_{\mathrm{LO}})t}\right] \\ Y &= \left[E_S(t-\tau)e^{-i(\omega_S-\omega_{\mathrm{LO}})(t-\tau)} + E_S^*(t-\tau)e^{i(\omega_S-\omega_{\mathrm{LO}})(t-\tau)}\right]\end{aligned} \tag{9}$$

In Equation (8) any exponential products containing *t* give zero after averaging, and only the exponents independent of *t* remain:

$$\left\langle i(t)i(t-\tau)\right\rangle_t = C_1^{\,2} + C_2^{\,2}\left[\left\langle E_S(t)E_S^*(t-\tau)\right\rangle e^{-i(\omega_S-\omega_{\mathrm{LO}})\tau} + \left\langle E_S^*(t)E_S(t-\tau)\right\rangle e^{i(\omega_S-\omega_{\mathrm{LO}})\tau}\right]. \tag{10}$$

Since we are averaging over t, t can be replaced with $(t+\tau)$ in the first term with angle brackets. Since this term represents signal field's auto-correlation function, which depends only on $|\tau|$, τ within these angle brackets can be replaced with $-\tau$, leading to

$$\langle i(t)i(t-\tau)\rangle_t = C_1^2 + 2C_2^2\langle E_S(t)E_S^*(t-\tau)\rangle\cos(\omega_S-\omega_{LO})\tau, \quad (11)$$

which shows that the auto-correlation of the signal's electric field can be straightforwardly obtained from the auto-correlation of the heterodyne photocurrent.

Auto-Correlation Function

Autocorrelation is the cross-correlation of a signal with itself. Physically, it quantifies the similarity between observations of a function at two time-separated instances. It is a mathematical tool for finding repeating patterns, such as the presence of a periodic signal which has been buried under noise, or identifying the duration of noise fluctuations [3]. For optical signal, the auto-correlation function is mathematically expressed as

$$g(\tau) = \langle E(t-\tau)E^*(t)\rangle, \quad (12)$$

where $g(\tau)$ is the auto-correlation function, τ – time delay, and $E^*(t)$ and $E(t-\tau)$ – electric fields in time domain with time delay. In Section 3, we will process beat photocurrent between two lasers that contains 60 million data points taken at 120 GSamples/s rate. The data cover time period t_{max} calculated as

$$t_{max} = 60\times10^6 \text{ Samples } / (120 \text{ GSamples/s }) = 500\,\mu\text{s}. \quad (13)$$

For calculation of $g(\tau)$, we use time delay $\tau = 0\ldots500\mu\text{s}$ with a step size of 10 original data samples, i.e., 10 / (120 GSamples/s) ≈ 83 ps.

Power Spectral Density

Power spectral density (PSD) function shows the strength of the signal variations as a function of frequency. In other words, it shows at which frequencies variations are strong and at which frequencies variations are weak [4]. The unit of PSD is power per unit frequency window (i.e., same units as energy), and you can obtain the power within a specific frequency range by integrating PSD over that frequency range. According to Wiener–Khinchin theorem, the computation of PSD can be done by taking a Fourier transform (FT) of the autocorrelation function. In the case of beat photocurrent, the autocorrelation function is multiplied by $a(t) = \cos[2\pi(\nu_S - \nu_{LO})t]$, a harmonic at the beat frequency (ν_S–ν_{LO}). Therefore, the PSD is a convolution of the FTs of the two factors:

$$\mathrm{PSD} = \mathrm{FT}\{g(\tau)\} * a(f) = G(f) * a(f), \tag{14}$$

where

$$a(f) = \frac{1}{2}\delta\left[f - (\nu_S - \nu_{LO})\right] + \frac{1}{2}\delta\left[f + (\nu_S - \nu_{LO})\right] \tag{15}$$

and

$$\mathrm{PSD} = \frac{1}{2}G\left[f - (\nu_S - \nu_{LO})\right] + \frac{1}{2}G\left[f + (\nu_S - \nu_{LO})\right]. \tag{16}$$

Since the RF spectra (especially on spectrum analyzers) are usually plotted by adding the powers PSD(f) + PSD($-f$) and are shown versus positive f, the observed spectrum directly corresponds to $G(f - |\nu_S - \nu_{LO}|)$, i.e., PSD of the signal shifted by $|\nu_S - \nu_{LO}|$.

On-Off Keying

On-off keying (OOK) is the simplest form of amplitude-shift keying (ASK) modulation format that represents digital data as the presence or absence of a carrier wave. In its simplest form, the presence of a carrier for a specific duration represents a binary one, while its absence for the same duration represents a binary zero. Some more sophisticated schemes vary these durations to convey additional information. It is analogous to unipolar encoding line code [5].

Return-to-zero

Return-to-zero (RZ) describes a line code used in telecommunications signals in which the signal drops (returns) to zero between each pulse. The "zero" between each bit is a neutral or rest condition, such as a zero amplitude in pulse amplitude modulation (PAM), zero phase shift in phase-shift keying (PSK), or mid-frequency in frequency-shift keying (FSK). For electrical signals, the "zero" condition is typically halfway between the significant condition representing a 1 bit and the other significant condition representing a 0 bit [6].

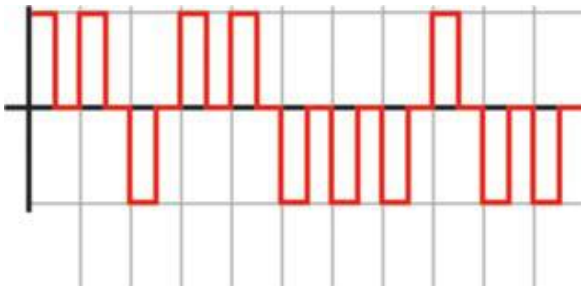

Figure 2.1: A binary signal encoded using rectangular pulse amplitude modulation with polar return-to-zero code (taken from Ref. [6]).

Non-return-to-zero

In telecommunication, a non-return-to-zero (NRZ) line code is a binary code in which 1s are represented by one significant condition (usually a positive voltage) and 0s are represented by some other significant condition (usually a negative voltage), with no other neutral or rest condition. The pulses have more energy than a RZ code. Unlike RZ, NRZ does not have a rest state. NRZ is not inherently a self-synchronizing code, thus some additional synchronization technique (for example a run length limited constraint, or a parallel synchronization signal) must be used for avoiding bit slip [6].

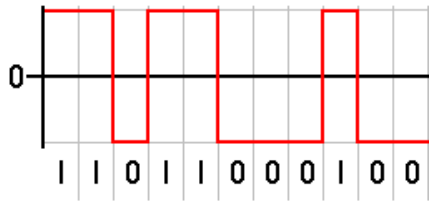

Figure 2.2: A binary signal encoded using rectangular pulse amplitude modulation with polar non-return-to-zero code (taken from Ref. [6]).

Chapter 3

Experiments and Results

The experiments involve beating of the DFB and the ANDO lasers where the DFB laser is the signal and the ANDO laser is the local oscillator. ANDO is an instrument-grade tunable external-cavity semiconductor laser with internal gas cell serving as a frequency reference. It has a narrow linewidth (~200 kHz) and stable frequency (< 100 MHz/hr drift). Hence, its frequency fluctuations can be neglected compared to those of the DFB laser.

Both lasers are not modulated

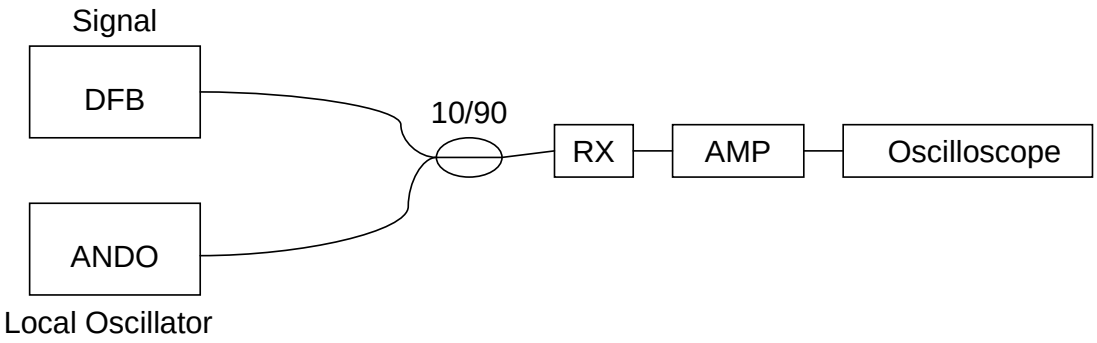

Figure 3.1: Schematic diagram of the experimental setup.

The schematic diagram of the first experiment is shown in Figure 3.1. Both lasers were not modulated, and were combined using a 10/90 coupler. The combined signal was received by one arm of Discovery Semiconductor balanced receiver with 18-GHz

bandwidth and amplified by a Picosecond Pulse Labs Ultra-Broadband Amplifier 5828A with 14-GHz bandwidth. The amplified signal was fed to a LeCroy WaveMaster 8 Zi-A series real-time oscilloscope with 120 GSamples/s sampling rate. With the help of this oscilloscope, photodetector output was recorded as a function of time, and the data was used for further analysis.

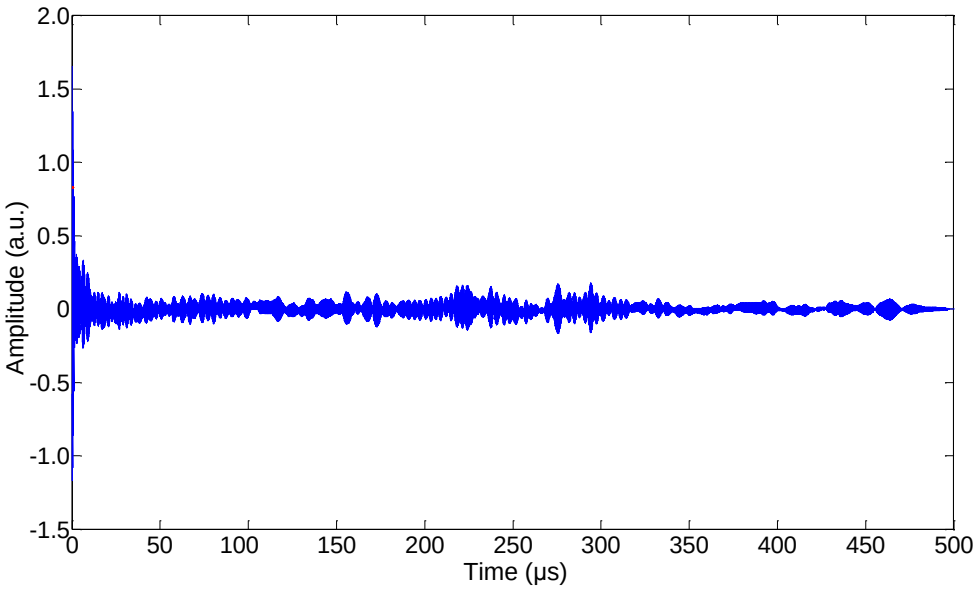

Figure 3.2: Auto-correlation function of the photocurrent.

With the data obtained from the oscilloscope, the auto-correlation function of the photocurrent was computed and plotted in Figure 3.2. Figure 3.3 zooms into the first 2 μs of the auto-correlation function, from which the Half-Wave at Half Maximum (HWHM) of the auto-correlation function τ_{HWHM} can be obtained. The HWHM is approximately $\tau_{HWHM} \approx 1$ μs.

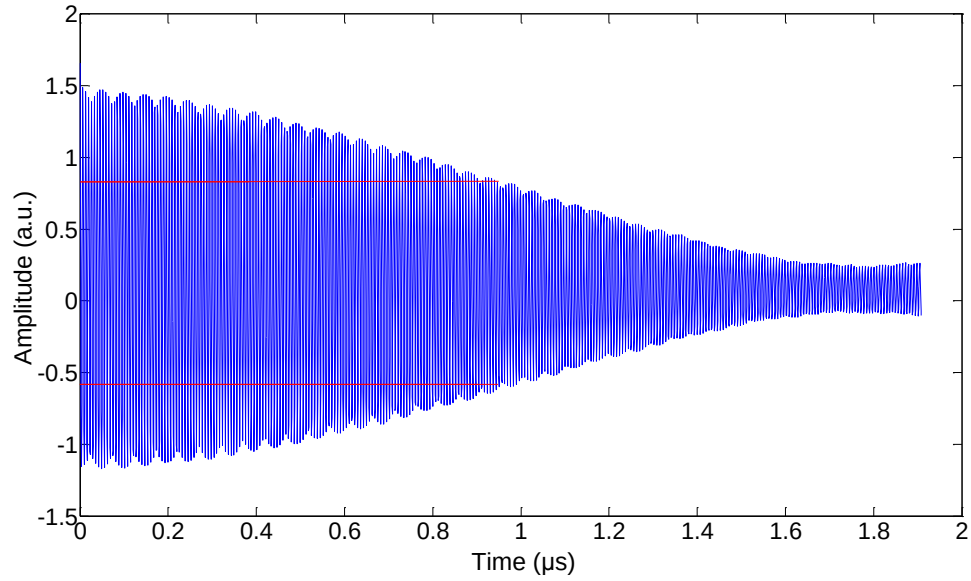

Figure 3.3: Expanded first 2 μs of the auto-correlation function.

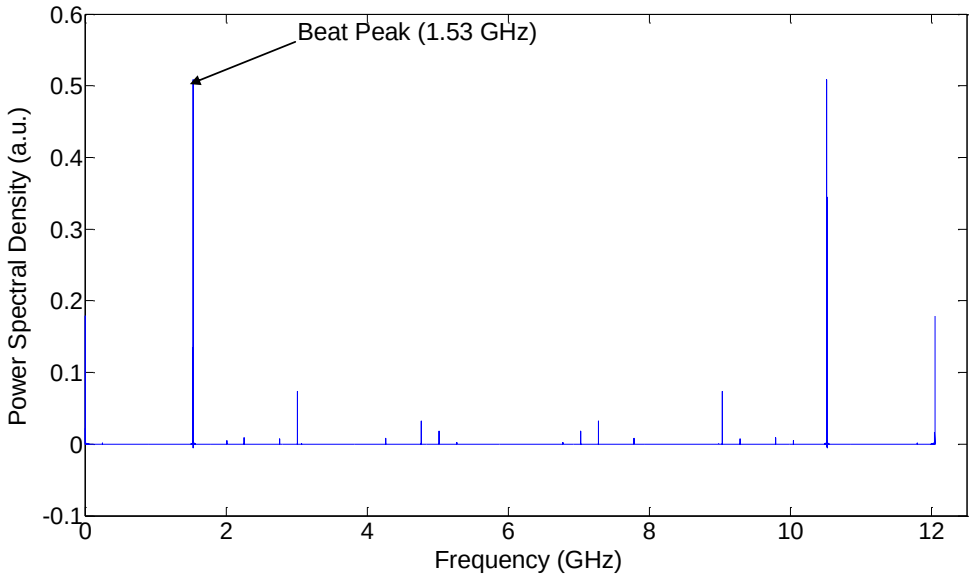

Figure 3.4: Fourier transform of the auto-correlation function.

As we discussed in the previous Chapter, Fourier transform of the auto-correlation function produces the power spectral density. Figure 3.4 displays the Fourier transform of the data shown in Figure 3.3. Due to the modulation of the auto-correlation function by the signal-LO beat frequency ($|\nu_S - \nu_{LO}| \approx 1.53$ GHz in this particular measurement), the power spectral frequency of the signal is centered around 1.53-GHz beat frequency.

Figure 3.5 shows a zoomed-in version of Figure 3.4 in the vicinity of the signal-LO beat frequency. This gives details on the beating between the two lasers. Figure 3.6 shows the data of Figure 3.5 on logarithmic scale. The noisy central part of the spectrum represents fluctuations of the DFB center frequency during the 500-μs acquisition time, whereas the spectral wings represent the Lorentzian lineshape of the natural DFB spectrum (Schawlow-Townes linewidth broadened by diode-laser's α-factor owing to the dependence of the refractive index on the carrier density) [7].

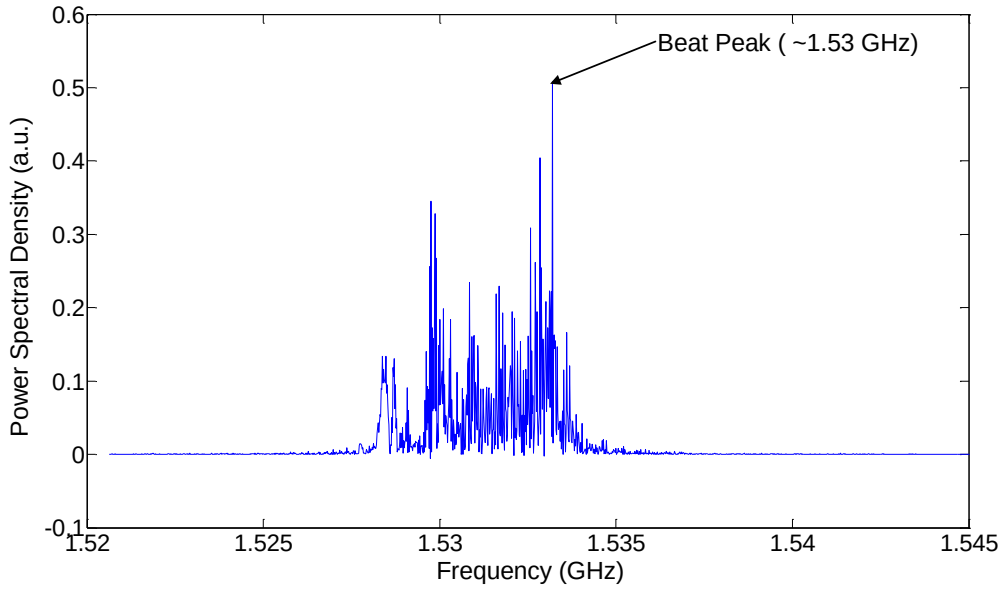

Figure 3.5: Data of Figure 3.4 in the vicinity of the signal-LO beat frequency.

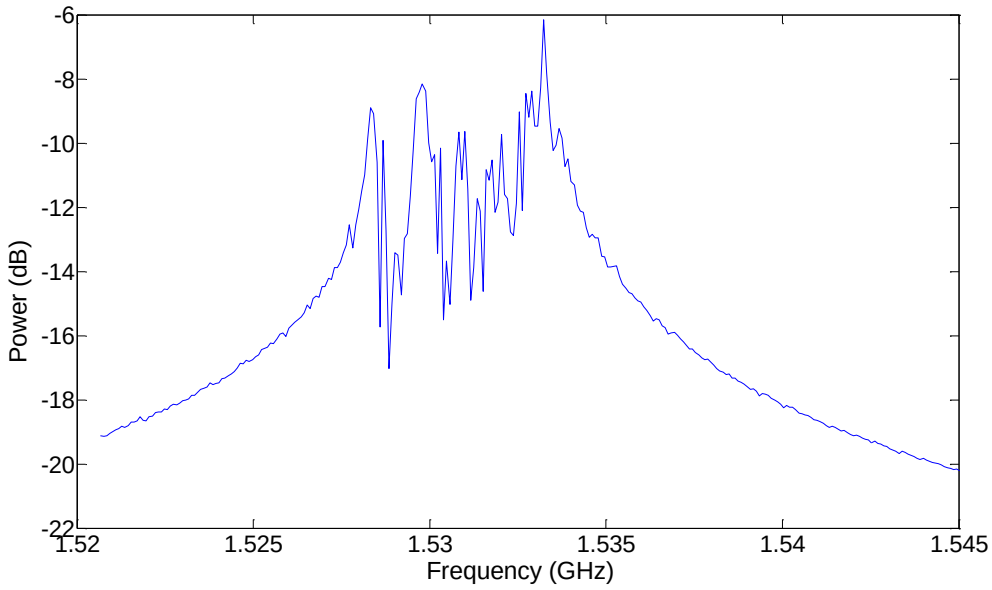

Figure 3.6: Data of Figure 3.4 on logarithmic scale.

In order to extract the natural width of the DFB laser spectrum, we fit the data with a superposition of two slightly offset Lorentzian lines given by

$$X = \frac{A_1}{1+\left(\frac{f-f_{0_1}}{\delta f/2}\right)^2} + \frac{A_2}{1+\left(\frac{f-f_{0_2}}{\delta f/2}\right)^2} + B, \qquad (17)$$

where A_1 and A_2 are the magnitudes on linear scale, B is the background noise level, f is the RF frequency, f_{0_1} and f_{0_2} are the center frequencies of two Lorentzians with full-width at half-maximum (FWHM) δf. By tweaking these parameters, a fairly close match was obtained which is shown in Figure 3.7. The inverse of the FWHM δf from the plot can be compared to the HWHM τ_{HWHM} of the auto-correlation function obtained from Figure 3, revealing agreement within a factor of 5:

$$\delta f \approx 5.1 \text{ MHz},$$

$$\left(\frac{1}{\delta f}\right) \approx 0.2\mu s \approx \tau_{HWHM}/5$$

Thus, the intrinsic linewidth of the DFB laser is 5.1 MHz.

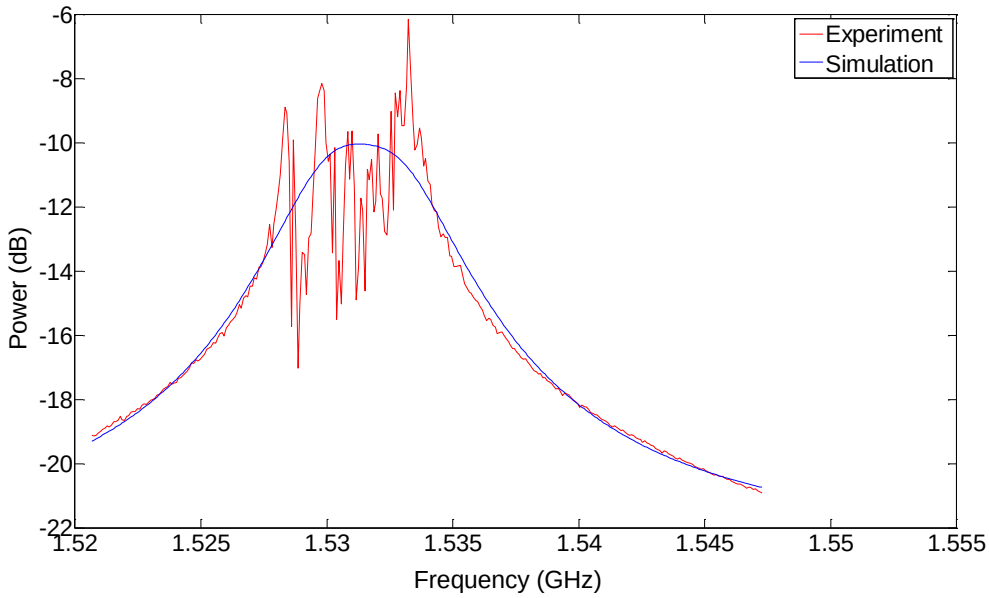

Figure 3.7: Fitting the data with a superposition of two Lorentzian curves.

While the previous data have been obtained by numerical processing of the time-domain data, the same conclusions can be reached from direct frequency-domain measurements when the oscilloscope is replaced with HP 8563A RF spectrum analyzer (26-GHz bandwidth).

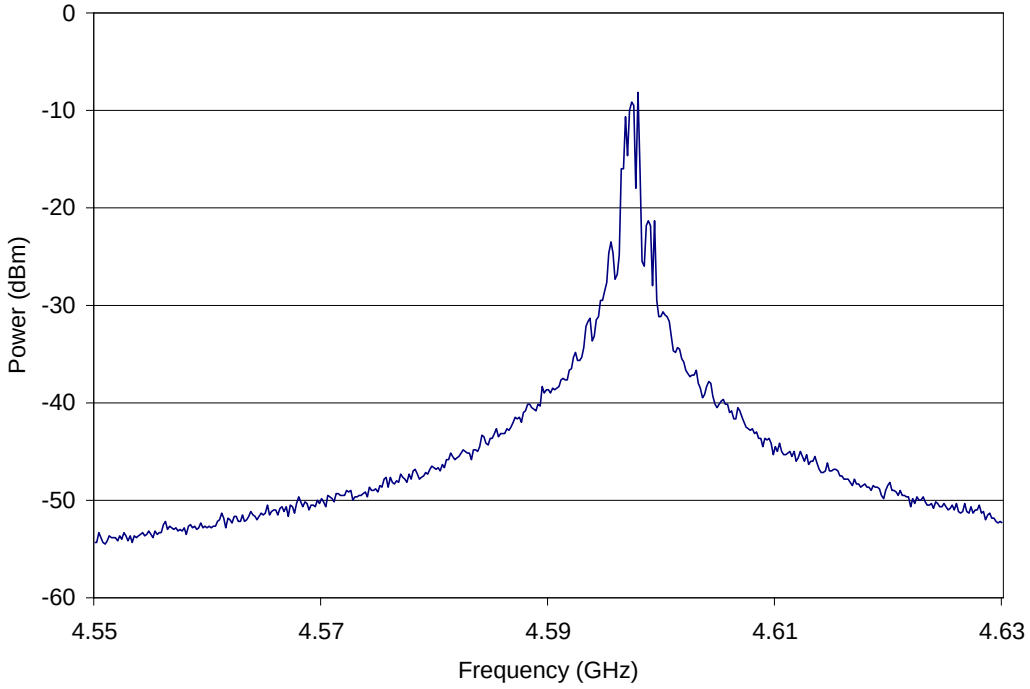

Figure 3.8: Beat note between the two lasers (both not modulated).

Figure 3.8 displays the beating spectrum between the DFB and the ANDO lasers when both of them are not modulated, demonstrating a lineshape similar to that in Figure 3.6 (only at a new center frequency, which has changed between the two experiments). What has become evident from the RF spectrum is the constantly moving center frequency of the beat note, owing to the technical (not intrinsic) fluctuations and drifts of the DFB frequency. Using a LabView script, we have recorded the position of the central peak every minute for several hours, which is shown in Figure 3.9. To separate the fast frequency fluctuations from large but slow drift, we have also computed and subtracted the 10-minute moving average of the frequency. The resulting drift (moving average) ranging between 12 MHz / hr and 76 MHz / hr is also shown in Figure 3.9, while the fast,

zero-mean fluctuations with standard deviation of ~6 MHz are shown in Figure 3.10, and their Gaussian-like histogram is shown in Figure 3.11. The slow drift is contributed by the drifts of both the signal and LO center frequencies.

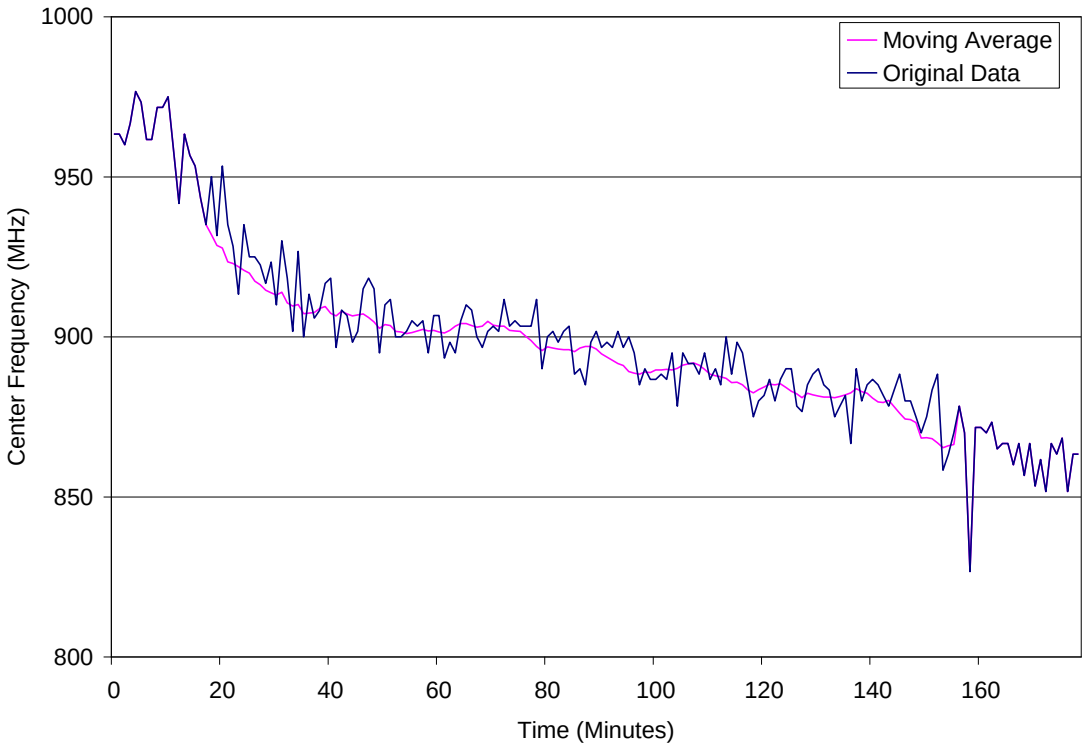

Figure 3.9: Fluctuations and drift of the beat frequency versus time.

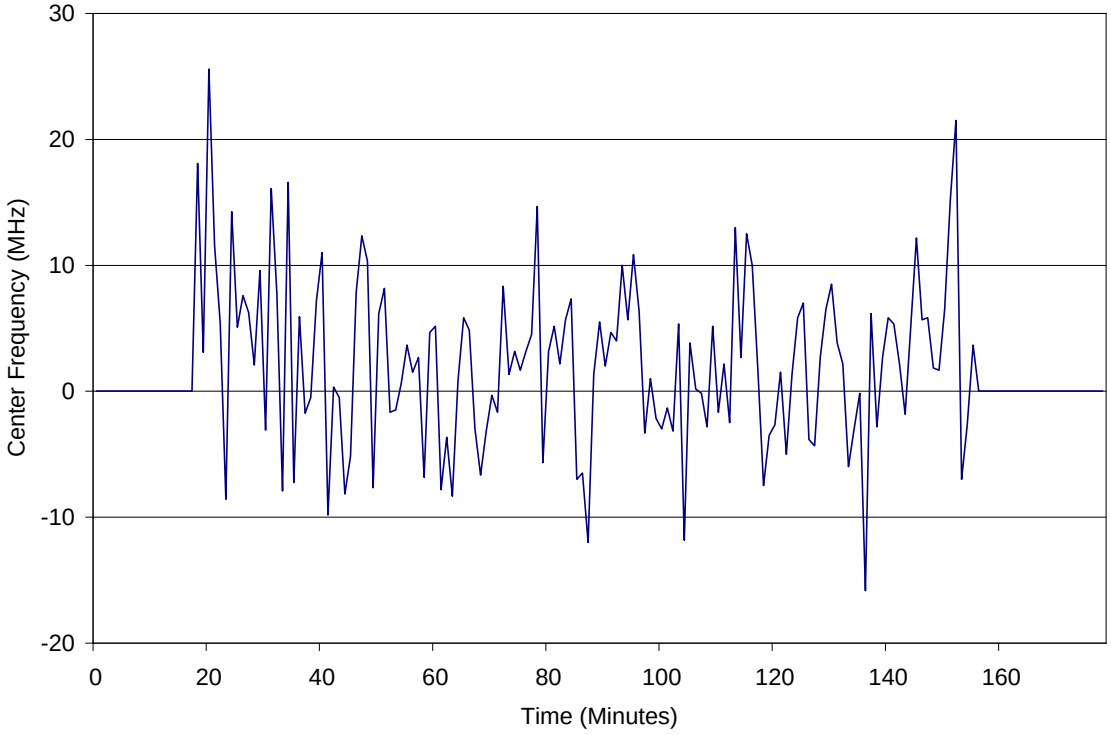

Figure 3.10: The fast, zero-mean fluctuations of the beat center frequency.

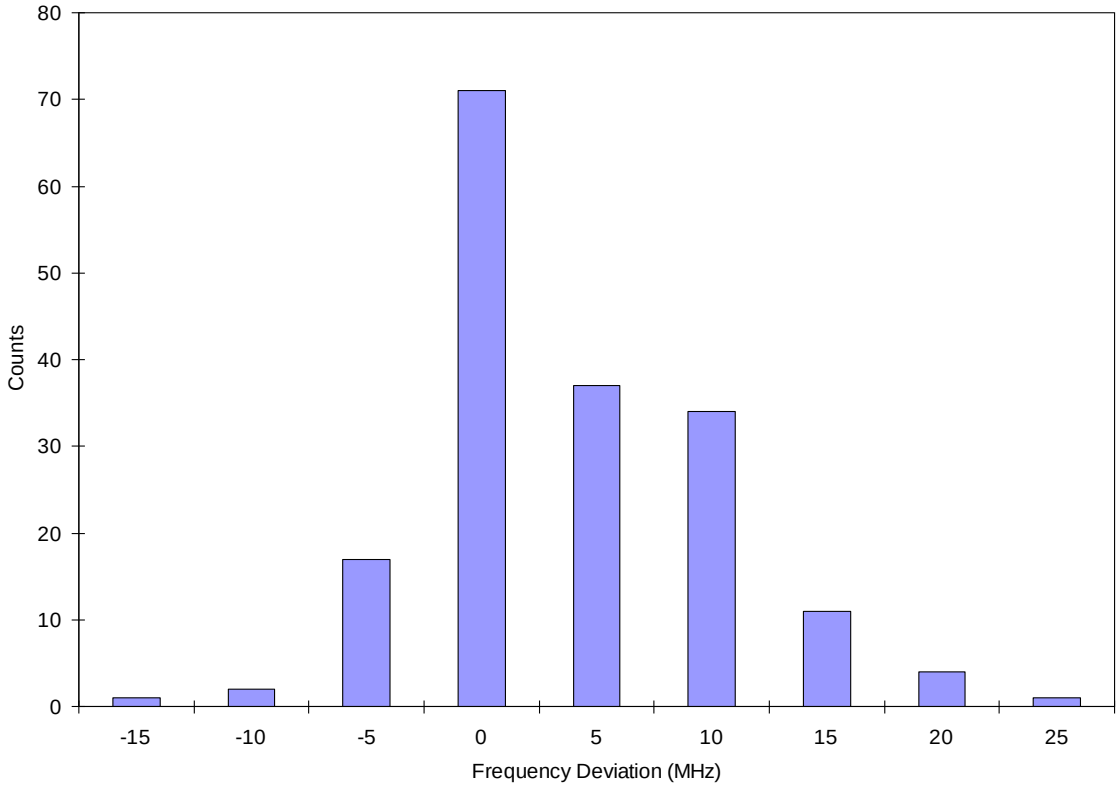

Figure 3.11: Histogram of the fast fluctuations of beat frequency.

Modulated DFB and continuous-wave local oscillator

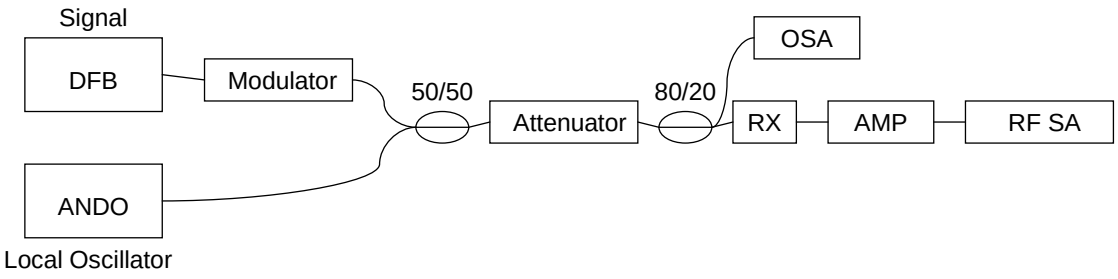

Figure 3.12: Experiment setup with modulated DFB laser.

The signal from the DFB laser is modulated by the modulator using On-Off Keying technique. The modulator produces either RZ- or NRZ-formatted pseudo-random bit sequence (PRBS) data at 10.79 Gb/s rate. The output form ANDO laser is combined with the DFB output from the modulator using a 50/50 coupler and is passed through an attenuator. The output from the attenuator is split using an 80/20 splitter: 20% of the power goes to ANDO AQ6317B optical spectrum analyzer (OSA) and 80% goes to the receiver (RX) that converts the optical signal to an electrical signal. The output from the RX is fed to an RF amplifier (RX and the amplifier are the same as those in the setup of Figure 3.1) and then sent to the RF Spectrum Analyzer (RF SA, HP 8563A). The lasers were made co-polarized by fiber polarization controllers (not shown).

In the first experiment, the modulator was set to RZ mode, the spectra were saved and documented for a) both lasers OFF, b) DFB ON, LO OFF, and c) both lasers ON. The spectra were observed on both optical spectral analyzer (for optical spectra; 0.01-nm resolution) and RF spectrum analyzer (for RF photocurrent spectra). Figure 3.13 shows the optical spectra and Figure 3.14 shows the RF spectra. The PRBS length was set to a value of $2^{31}-1$.

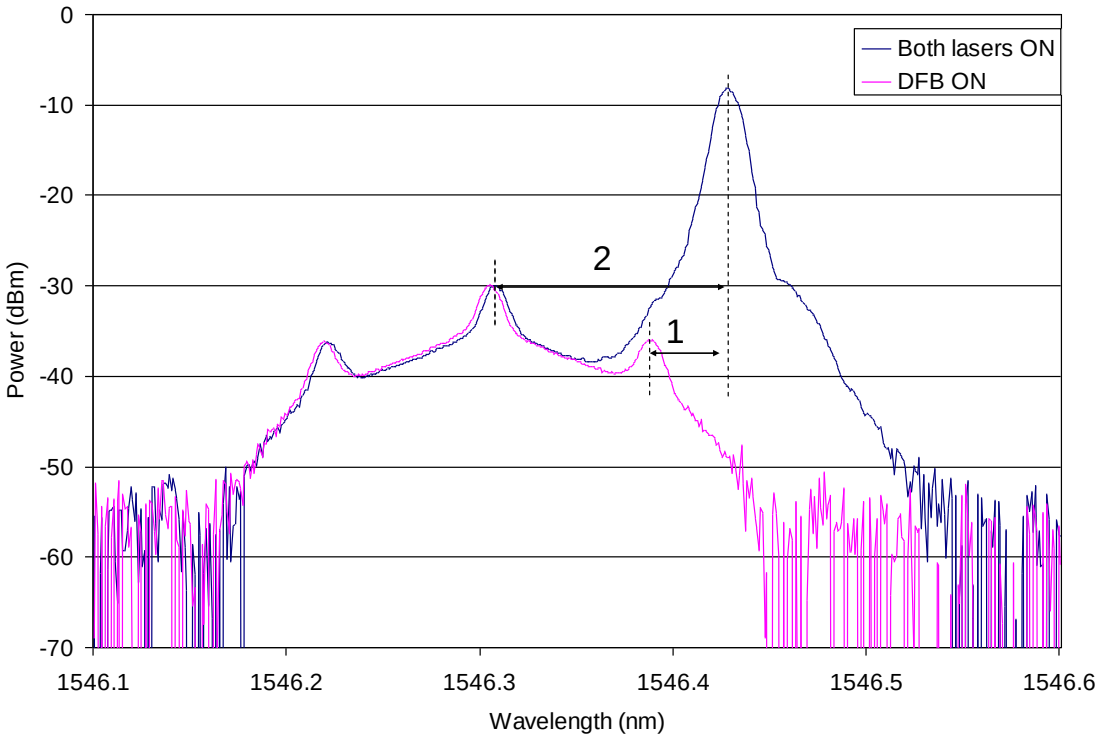

Figure 3.13: Optical spectra for RZ-modulated case.

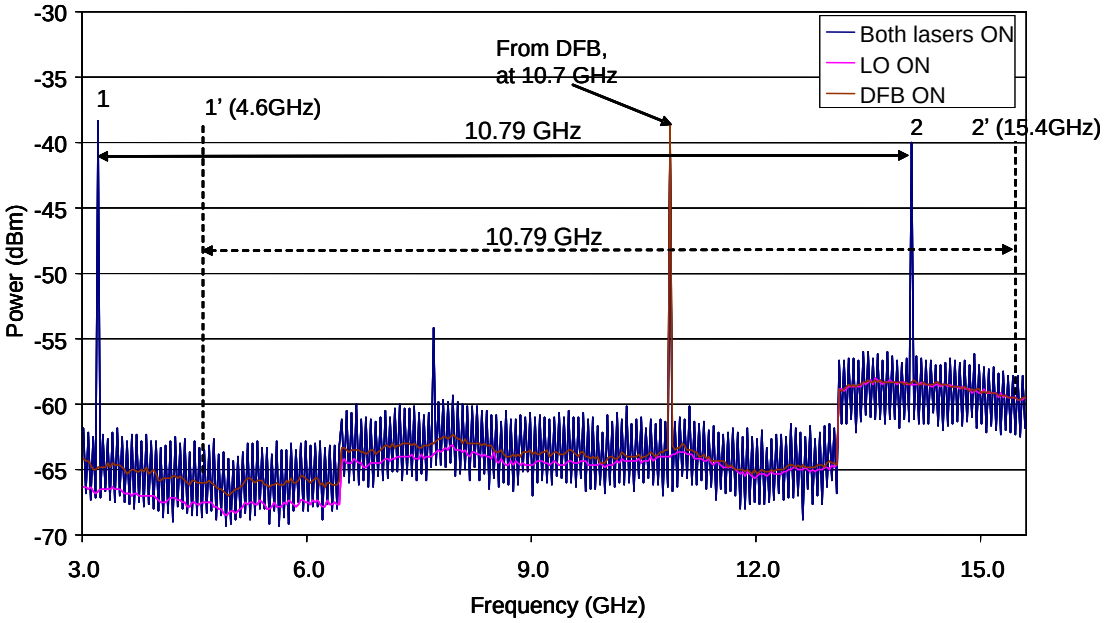

Figure 3.14: RF Spectra for RZ-modulated case. Peak labels correspond to the beatings between LO and DFB tones marked in Figure 3.13.

The peak observed at 10.79 GHz in Figure 3.14 comes from direct detection of the modulated DFB laser (first harmonic of the clock frequency). This is confirmed by the peak's presence even when the LO laser is OFF. Peak labels in Figure 3.14 correspond to the beatings between LO and DFB tones marked in Figure 3.13; peak 2 is the beating between the LO and the DFB carrier frequency; peak 1 is the beating between the LO and the right sideband of the DFB clock's first harmonic. Peaks 1 and 2 are separated by the clock frequency of 10.79 GHz and are observed only when both DFB and LO lasers are ON.

Before proceeding with next, higher-resolution RF spectrum measurements, the DFB laser was briefly turned off and on again. This resulted in a 0.012-nm (1.4-GHz) shift in the wavelength (frequency) of the DFB laser, and therefore the detuning between the two lasers changed. The new locations of peaks 1 and 2 are shown in Figure 3.14 as 1′ and 2′. Figures 3.15 and 3.16 show the zoomed-in view of the peak 2′ at 15.4GHz for PRBS lengths of 2^{31}–1 and 2^{7}–1, respectively.

The resolution bandwidth and the video bandwidth in the RF spectrum analyzer were set to 2 MHz and 10 KHz, respectively. The noisy trace in Figure 3.15 shows that the frequency was changing while the trace was being drawn.

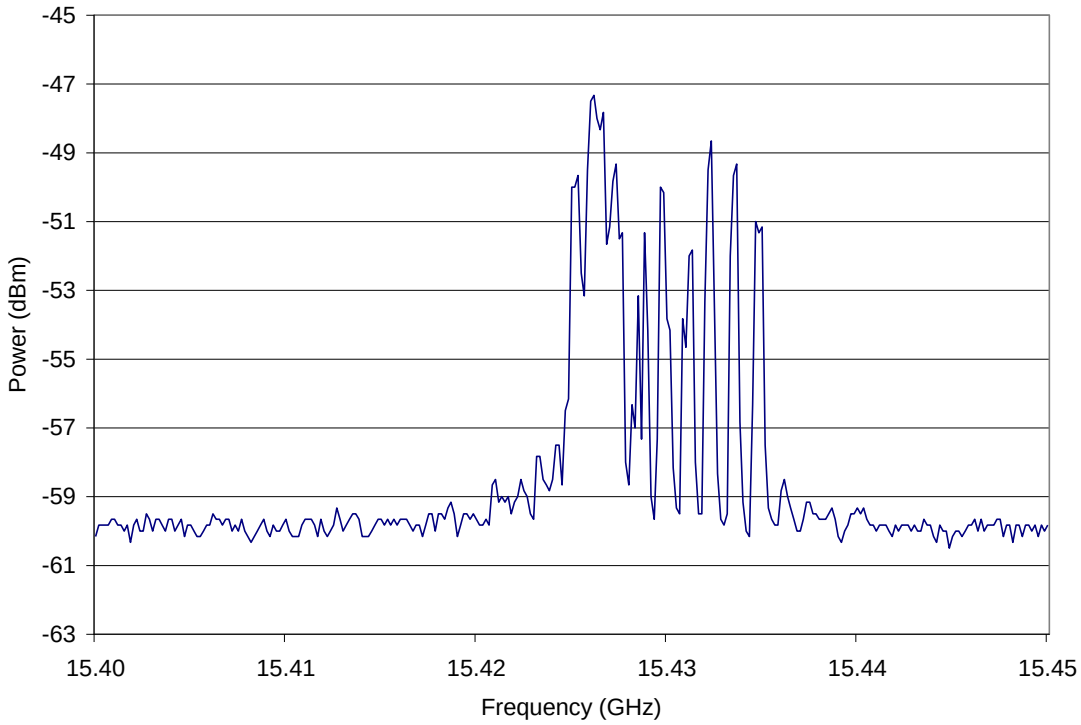

Figure 3.15: Beat peak 2′ at 15.43 GHz for PRBS length of 2^{31}–1.

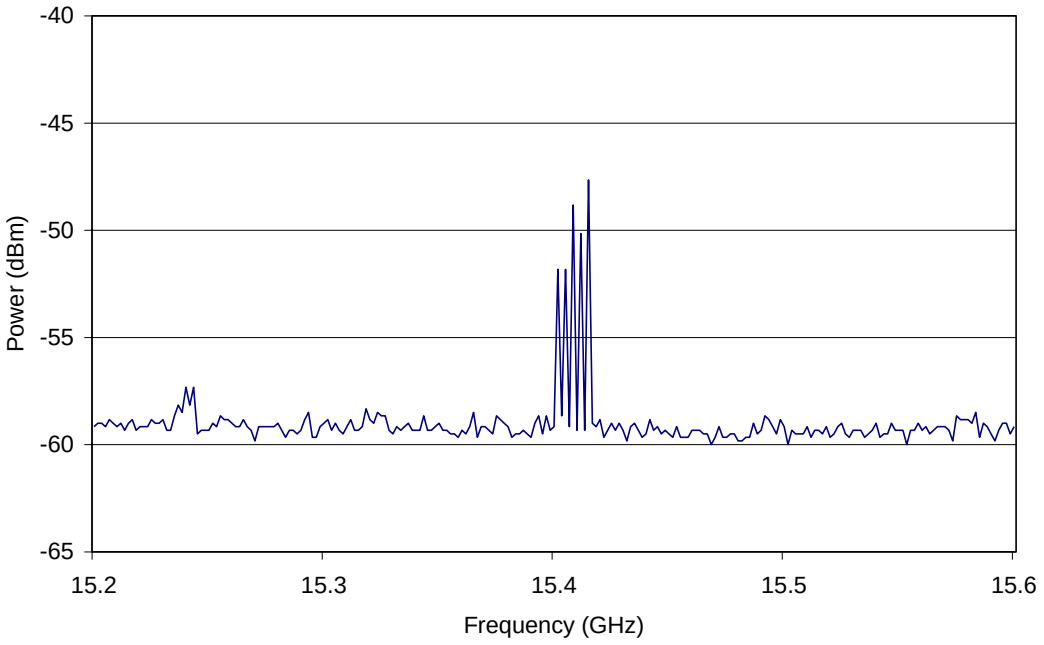

Figure 3.16: Beat peak 2′ at 15.43 GHz for PRBS length of 2^7–1.

Similarly, zoomed-in views of peak 1′ at 4.6 GHz are shown in Figures 3.17 and 3.18 at for PRBS lengths 2^{31}–1 and 2^7–1, respectively. The wide and noisy nature of peaks indicates the fluctuations of beat frequency during the trace acquisition time. As expected, the peak width is similar to that in the non-modulated case.

Unlike true data, the PRBS patterns are periodic, and their spectra consist of frequency combs with spacing equal to the PRBS repetition rate, i.e., the clock rate divided by the PRBS length. For 2^{31}–1 length, the repetition rate is 5 Hz, which is well below the resolution of the RF spectrum analyzer. As a result, outside of the clock harmonics, the spectrum for PRBS 2^{31}–1 looks continuous, with very low PSD almost indistinguishable from noise. On the other hand, for 2^7–1 PRBS length, the repetition rate

is ~84 MHz, which is easily resolved in Figure 3.17, showing two sets of 84-MHz-spaced frequency combs: one with narrow peaks, originating from the direct-detected DFB signal, and the other one with noisy peaks, originating from the beating between the DFB and LO. The 84-MHz-spaced peaks are not visible at 15.4 GHz (Figure 3.16), because at such a high frequency the RF signal is greatly attenuated by the combined amplitude responses of the detector and amplifier, and these peaks are comparable to the noise level.

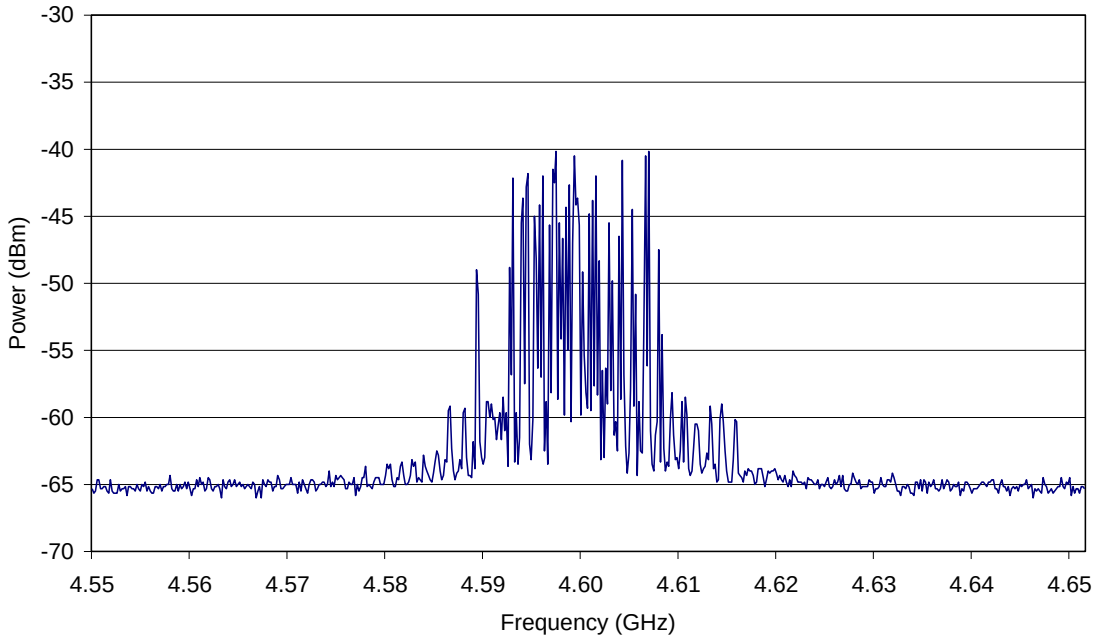

Figure 3.17: Beat peak 1′ at 4.6 GHz for PRBS length of 2^{31}–1.

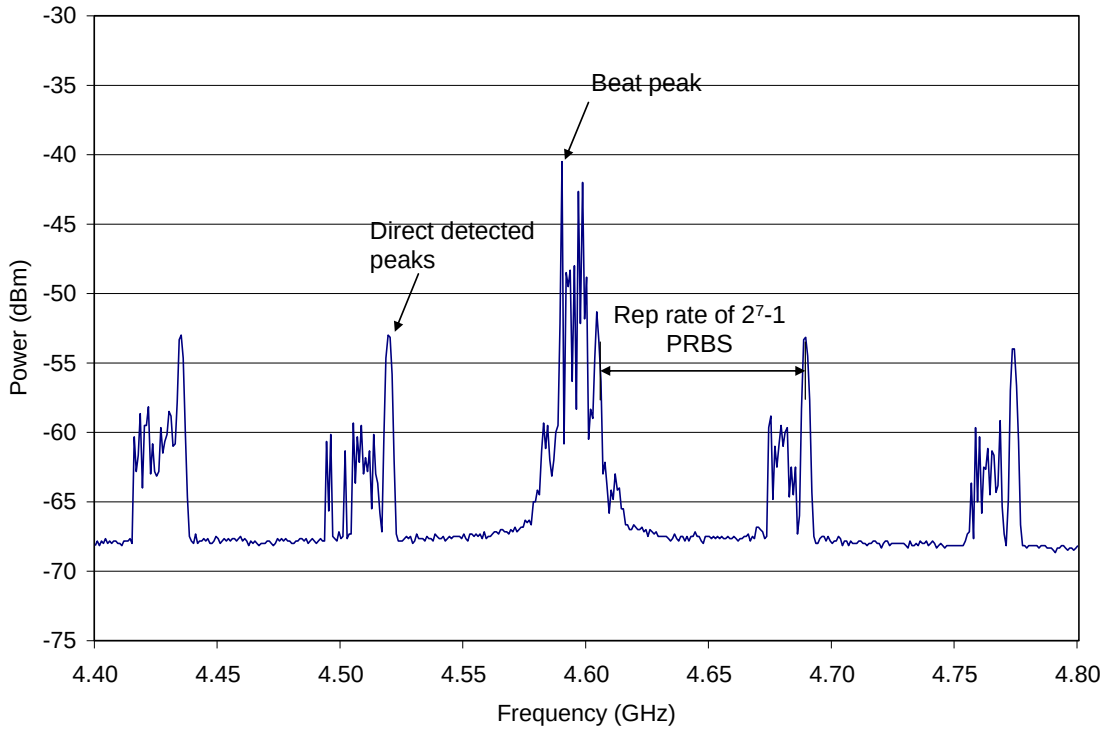

Figure 3.18: Beat peak 1′ at 4.6 GHz for PRBS length of 2^7–1.

In the next experiment, the modulator was set to NRZ mode, and the set of measurements similar to the RZ case was repeated, as shown in Figures 3.19–3.21.

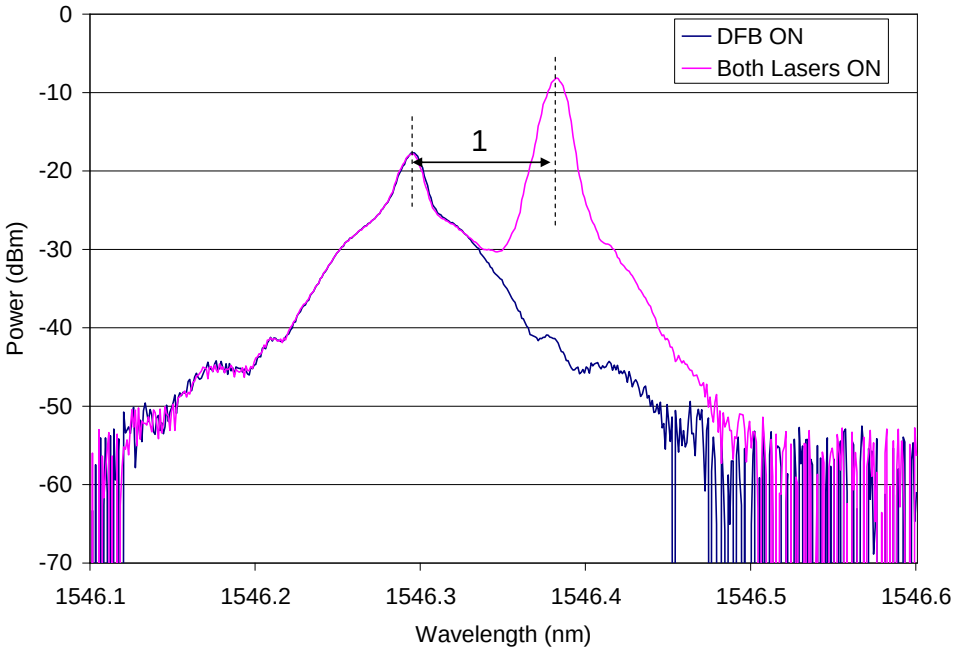

Figure 3.19: Optical Spectra for NRZ-modulated case. Peak label corresponds to the beating between LO and DFB tones marked in Figure 3.20.

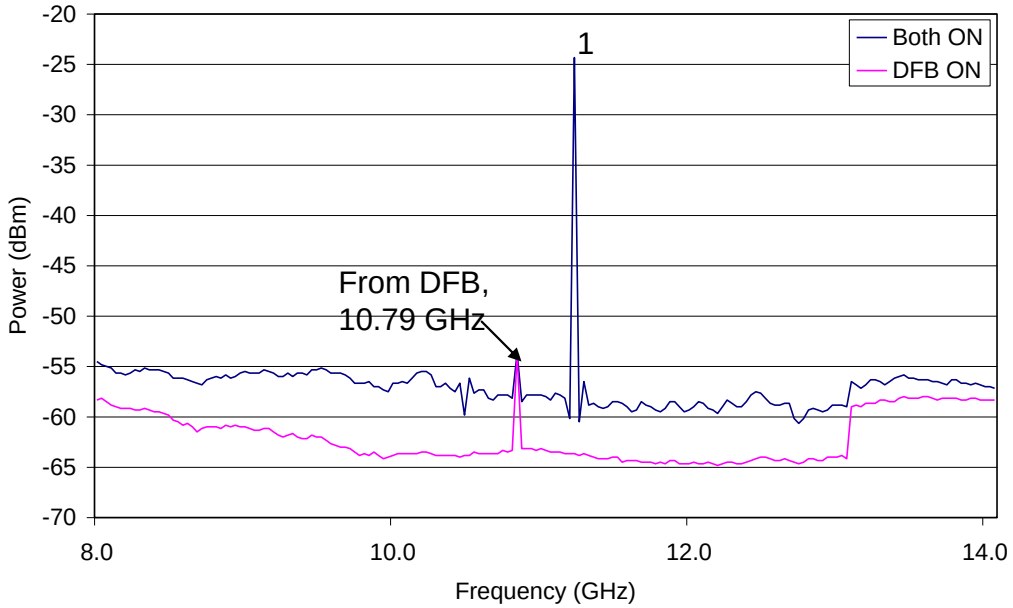

Figure 3.20: RF spectra for NRZ-modulated case.

The beating between the DFB carrier frequency and LO marked as 1 in Figure 3.20 corresponds to the peak 1 in Figure 3.19. NRZ spectrum does not contain the harmonic at clock frequency. The second peak at 10.79 GHz in Figure 3.20 is obtained by direct detection of the DFB signal. The PRBS was set at 2^{31}–1 for Figures 3.19 and 3.20. Figure 3.21 shows the 11.21-GHz beat frequency for NRZ obtained at PRBS length of 2^{7}–1.

Thus, the data obtained from continuous-wave, RZ- and NRZ-modulated cases all demonstrate the modulation-specific spectra broadened by the same frequency fluctuations arising from the intrinsic DFB linewidth, as well as from the slow drift and fast variations of the DFB center frequency.

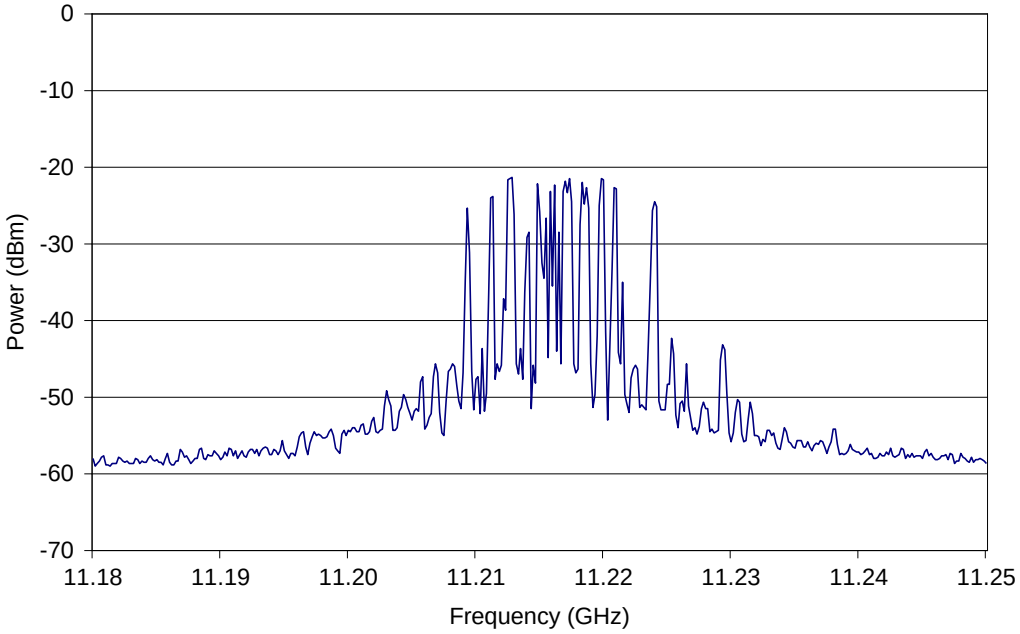

Figure 3.21: Beat peak 1 at 11.21 GHz for PRBS length of 2^7–1.

Chapter 4

Conclusion

The spectral properties of the DFB laser were experimentally analyzed for modulated and non-modulated cases by beating it with a local-oscillator laser. We compared the spectral data obtained from the photocurrent auto-correlation function, as well as from the RF and optical spectra.

The photocurrent beat peak was identified in the FFT of the auto-correlation plot, and the power spectral density was obtained by applying Fast Fourier Transformation for the auto-correlation data. A detailed plot of the beat peak in the FFT was done in order to elaborate the detail on different peaks and compared with theoretical model. From fitting the theoretical model to the spectral wings of the peak, the intrinsic linewidth of the DFB laser was found to be $\delta f \approx 5.1$ MHz. The width of the auto-correlation function's HWHM is of the same order as the $1/\delta f$ value. The HWHM was observed at approximately 1 μs and the $1/\delta f$ is about 0.2 μs.

The drift in the beat frequency was obtained by recording the beat frequency over a period of time. The moving average of the drift in the beat frequency was plotted, and the drift was found to be in the range of values between 12 MHz / hr and 76 MHz / hr. This drift, contributed by the drifts of both the signal and LO center frequencies, is accompanied by fast (time scale of ~ 1 min.) zero-mean fluctuations of the signal's center frequency with standard deviation of approximately 6 MHz.

With DFB laser modulated using On-Off-Keying and ANDO laser un-modulated, experiments were done with both RZ and NRZ mode with PRBS values 2^7-1 and 2^{31}-1.

The optical and RF spectrum were compared and the beatings of the LO with DFB carrier and first harmonic of the clock were identified. The RF spectrum has also shown the repetitive nature of the PRBS pattern.

The obtained data will be helpful in designing means of mitigating the frequency deviations of the DFB laser, e.g., an optical filter that converts frequency fluctuations to intensity and feeds them back to correct the DFB central frequency.

References

1. http://www.rp-photonics.com/linewidth.html.
2. Complete Laser Spectral Characterization, Brian Samoriski, PhD, Bristol Instruments Inc. http://www.photonics.com/Article.aspx?AID=46771
3. John G. Proakis, Dimitris G. Manolakis, *Digital Signal Processing: Principles, Algorithms, and Applications*, 2nd edition, Simon & Schuster Books For Young Readers, 1992.
4. http://www.cygres.com/OcnPageE/Glosry/Spec.html.
5. Muthana Y. A., S.A. Aljunid, R. Badlishah Ahmad, Hilal A. Fadhil, " Bit error rate (BER) performance of return-to-zero and non-return-to-zero data signals optical code division multiple access (OCDMA) system based on AND detection scheme in fiber-to-the-home (FTTH) networks", *Optica Applicata, Vol. XLI, No. 1, 2011.*
6. John Proakis, *Digital Communications*, 4th edition(2000), McGrawHill.
7. C. H. Henry, "Theory of the linewidth of semiconductor lasers," IEEE J. Quantum Electron. **18**, 259–264 (1982).

Biographical Information

Gokul Krishna Srinivasan received his B.Tech in Electrical and Electronics Engineering form SRM Institute of Science and Technology-Chennai, India. He is interested in physics and concepts involved in optics. Gokul is a wildlife photographer by passion and he also enjoys playing music.